Ceramics International xxx (xxxx) xxx–xxx

Contents lists available at ScienceDirect

Ceramics International

journal homepage: www.elsevier.com/locate/ceramint

Infiltrated $La_{0.5}Ba_{0.5}CoO_{3-\delta}$ in $La_{0.8}Sr_{0.2}Ga_{0.8}Mg_{0.2}O_{2.8}$ scaffolds as cathode material for IT-SOFC

C. Setevich[a,*], S. Larrondo[a,b], F. Prado[c]

[a] UNIDEF, MINDEF, CONICET, Departamento de Investigaciones en Sólidos, CITEDEF, J.B. de La Salle 4397, 1603 Villa Martelli, Pcia. de Buenos Aires, Argentina
[b] Instituto de Investigación e Ingeniería Ambiental, UNSAM, Campus Miguelete, 25 de Mayo y Francia, 1650 San Martín, Pcia. de Buenos Aires, Argentina
[c] Departamento de Física, Universidad Nacional del Sur and IFISUR, CONICET, 8000 Bahía Blanca, Argentina

ARTICLE INFO

Keywords:
Infiltration
Mixed ionic–electronic conductors
LBC cathode
LSGM electrolyte
SOFC

ABSTRACT

The electrochemical response of infiltrated $La_{0.5}Ba_{0.5}CoO_{3-\delta}$ (LBC) in porous $La_{0.8}Sr_{0.2}Ga_{0.8}Mg_{0.2}O_{2.8}$ (LSGM) has been investigated. The thermal expansion coefficient (TEC) of the resulting electrode was measured, obtaining $\alpha = 12.5 \times 10^{-6}\ K^{-1}$, a value similar to that of LSGM. The polarization resistance (*Rp*) and the processes involved in the oxygen reduction reaction (ORR) for the new electrode were studied and analyzed through complex impedance spectroscopy measurements as a function of temperature and oxygen partial pressure (pO_2), using a symmetrical cell. The value of Rp for the infiltrated LBC turned out to be lower than that measured for an electrode prepared with a composite LBC-LSGM (1:1 wt%) by an order of magnitude, for the temperature range 750 °C ≤ T ≤ 900 °C, and about 5 times lower for the temperature range 450 °C ≤ T ≤ 650 °C. At 600 °C, the LBC infiltrated cathode exhibits a polarization resistance $R_p = 0.22\ \Omega\,cm^2$, in air. The complex impedance spectra show two processes, one identified as low frequency (LF),with a characteristic frequency of 10 Hz, and the other as intermediate frequency (IF), with a range between 0.05 and 2000 Hz. The LF process could be associated to the diffusion of oxygen in the gas phase through the pores of the electrode. Its resistance, $R_{LF} = 0.01\ \Omega c\,m^2$, was found to be independent of the temperature and half of that obtained for the LBC composite cathode. On the other hand, the IF process is related to charge transfer at the electrode surface and the electrode-electrolyte interface. The LBC cobaltite infiltrated in the LSGM scaffolds offers an adequate thermal expansion coefficient and good electrocatalytic activity for the ORR.

1. Introduction

Solid oxide fuel cells (SOFCs) are highly efficient electrochemical devices that convert chemical energy from fuel into electrical energy. They are mainly formed by the ensemble of three different oxides, the cathode, where the oxygen reduction reaction (ORR) takes place, the electrolyte and the anode, where fuel is oxidized [1]. Traditionally SOFCs operate at high temperatures, 800 °C ≤ T ≤ 1000 °C, which allows the use of unreformed hydrocarbon as fuels. However, in order to become economically competitive, the operating temperature for SOFC devices should be lowered to an intermediate range, 500 °C ≤ T ≤ 800 °C. This will reduce sealing and degradation problems, chemical reactions between cell components and will allow the use of cheaper materials, such as stainless steel, as interconnector material [2]. It will also improve the response in the on-off cycles between the ambient and the operating temperature. On the other hand, the polarization resistance of the cell components increases with decreasing temperature, deteriorating the cell performance, especially in the case of the cathode [2,3].

Among cathode materials proposed for intermediate temperature, mixed conductors oxides (MIEC) with the ABO_3 perovskite structure, containing rare or alkaline earth in the A site and cobalt in the B site, have presented low polarization resistance (Rp) values [4–6]. In particular, the oxide with composition $La_{0.5}Ba_{0.5}CoO_{3-\delta}$ (LBC) with cubic or double perovskite structure has low polarization resistance values, structural stability and good chemical compatibility with the electrolyte material [7–12]. When LBC oxide is used as cathode with $La_{0.8}Sr_{0.2}Ga_{0.8}Mg_{0.2}O_{2.8}$ (LSGM) as electrolyte, chemical compatibility up to 1100 °C was observed and power density values greater than 500 mW/cm^2 were obtained for the system anode/LSGM/LBC [13]. On the other hand, as previously reported [7], the LBC oxide presents a thermal expansion coefficient (TEC) of $\alpha \approx 25 \times 10^{-6}\ K^{-1}$, much larger than that of LSGM (which have a TEC value $\alpha \approx 12 \times 10^{-6}\ K^{-1}$) or Gd doped ceria (GDC) usually proposed as electrolyte material in intermediate temperature SOFCs (IT-SOFCs). This TEC mismatch results in poor adhesion and degradation problems which grow worse with

* Corresponding author.
E-mail address: cmartinez@citedef.gob.ar (C. Setevich).

https://doi.org/10.1016/j.ceramint.2018.06.121
Received 22 March 2018; Received in revised form 28 May 2018; Accepted 14 June 2018

temperature cycles. In order to reduce this difference, a mixture of the electrolyte and LBC materials can be used to form either composites [8,11] or compositionally graded cathodes [9]. In this last configuration, the electrode composition gradually changes from that of the electrolyte to the one corresponding to cathode material [7,9,14]. Another way of decreasing the difference in TEC values between cathode and electrolyte is to prepare an electrode by infiltrating the cathode material into a skeleton of the electrolyte material [15,16]. Several infiltration processes have been successfully developed and have shown to improve the performance and stability of the SOFC cell [17–20]. The utilization of an infiltrated electrode reduces the TEC mismatch, allows control of the particle size by selecting the calcination temperature [21], avoids reactivity between the electrode and the electrolyte if a low heat treatment temperature (400–1000 °C) is used [22], increases the electrode-electrolyte charge transfer surface compared to that corresponding to an electrode deposited on a flat electrolyte surface and, finally, thin dense electrolytes (< 50 μm) can be prepared by a simple technique, such as co-pressing, in which the skeleton is used as support [23].

The performances of infiltrated electrodes, the processes involved during the ORR and the deterioration of the cathode performance over time are usually studied by complex impedance spectroscopy measurements in symmetrical cells. Wang et al. [24] observed that the polarization resistance due to charge transfer processes at gas/electrode surface and electrode/electrolyte interfaces in double perovskite $PrBaCo_2O_{3-\delta}$ (PBC) infiltrated in $Ce_{0.9}Sm_{0.1}O_{1.95}$ (SDC) was lower than that observed in a PBC + SDC composite electrode [25]. Han et al. [26] identified three limiting processes in a cathode prepared with $SmBa_{0.5}Sr_{0.5}Co_2O_{5+\delta}$ (SBSC) infiltrated in a LSGM backbone: a) the charge transfer in the electrode-electrolyte interface, b) the charge transfer at the SBSC surface and c) the oxygen molecule diffusion in the gas phase, corresponding to the high, medium and low frequency ranges, respectively. In this case, the largest polarization resistance was obtained for the electronic charge transfer to adsorbed oxygen atoms on the electrode surface.

Previous studies of our group on LBC electrodes prepared as a composite with GDC [8] or as a graded cathode [9], have yielded a very low polarization resistance value, $Rp \sim 0.075\ \Omega\ cm^2$ at 600 °C, which is close to the lowest values reported in the literature [3]. Thus, based on these positive results and considering the advantages of the infiltration technique we prepared electrodes by infiltrating LBC in LSGM scaffolds in order to evaluate their electrochemical performances as cathodes for the ORR. The cathode response was evaluated by electrochemical impedance measurements on symmetrical cells as a function of temperature and oxygen partial pressure (pO_2). The limiting processes of the ORR were analyzed and identified. The performance of the infiltrated LBC electrode was compared with that corresponding to an electrode prepared with a composite of LBC + LSGM.

2. Experimental

LSGM powder was prepared by solid-state reaction using required amounts of La_2O_3, previously dried overnight at 1000 °C, $SrCO_3$, Ga_2O_3 and MgO. Raw materials were mixed using a jar mill with ethanol and 5 mm diameter ZrO_2 balls during 8 h and then calcined at 1000 °C for 12 h. The resulting powder was milled for 24 h and calcined at 1400 °C for 24 h in air. This procedure was performed twice. The cobaltite LBC was prepared by solid state reaction following the procedure previously reported [7]. The electrodes of the symmetrical cells for impedance spectroscopy measurements were prepared infiltrating the LBC precursor solution into the porous LSGM skeleton. The cell with the porous/dense/porous electrolyte configuration was fabricated using the co-pressing technique. The electrode skeletons were prepared mixing soluble starch as pore former with LSGM in a 40:60 wt% ratio in isopropyl alcohol using a agate mortar. The three electrolyte layers starch + LSGM/LSGM/starch + LSGM were pressed uniaxially at 100 MPa and

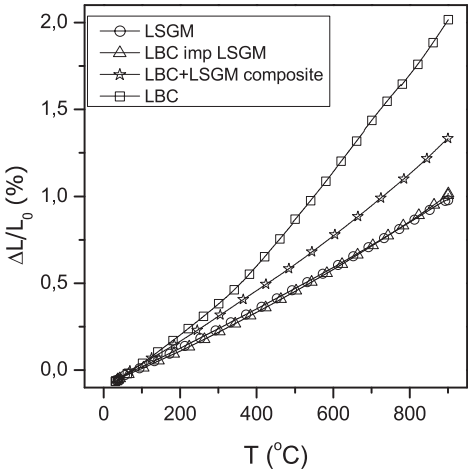

Fig. 1. Relative length change $\Delta L/L_0$ as a function of temperature for LBC, composite LBC + LSGM, infiltrated LBC in LSGM backbone and dense LSGM.

Table 1
TEC values.

	T (°C)		
	100–350	400–900	100–900
LBC	20.3	29.3	26.4
Composite	13.9	17.4	16.2
Infiltrated	10.6	13.7	12.5
LSGM	11.1	12.5	12.0

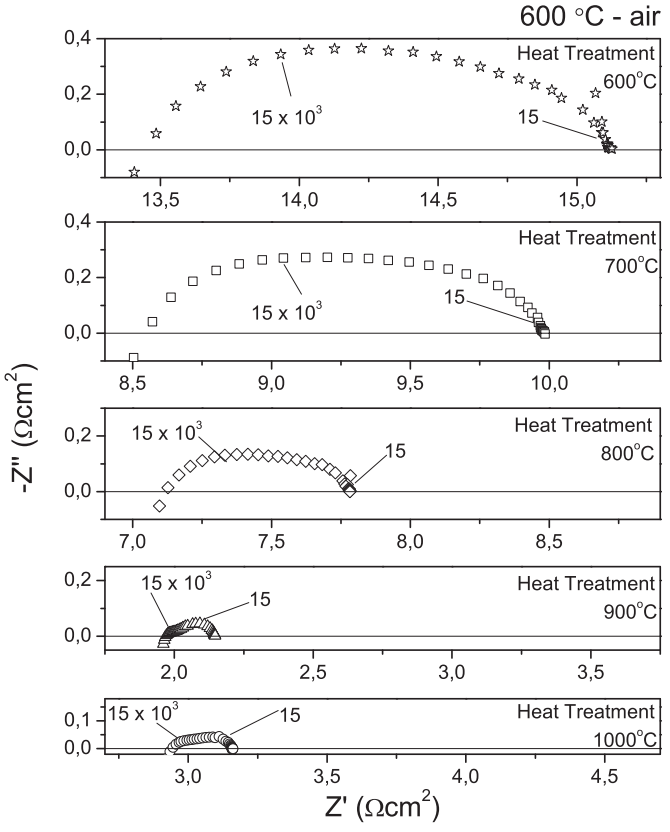

Fig. 2. Complex impedance spectra for infiltrated LBC electrodes. These impedance spectra were measured at T = 600 °C, in ambient air, after the electrode was heat treated at various temperatures between 600 and 1000 °C.

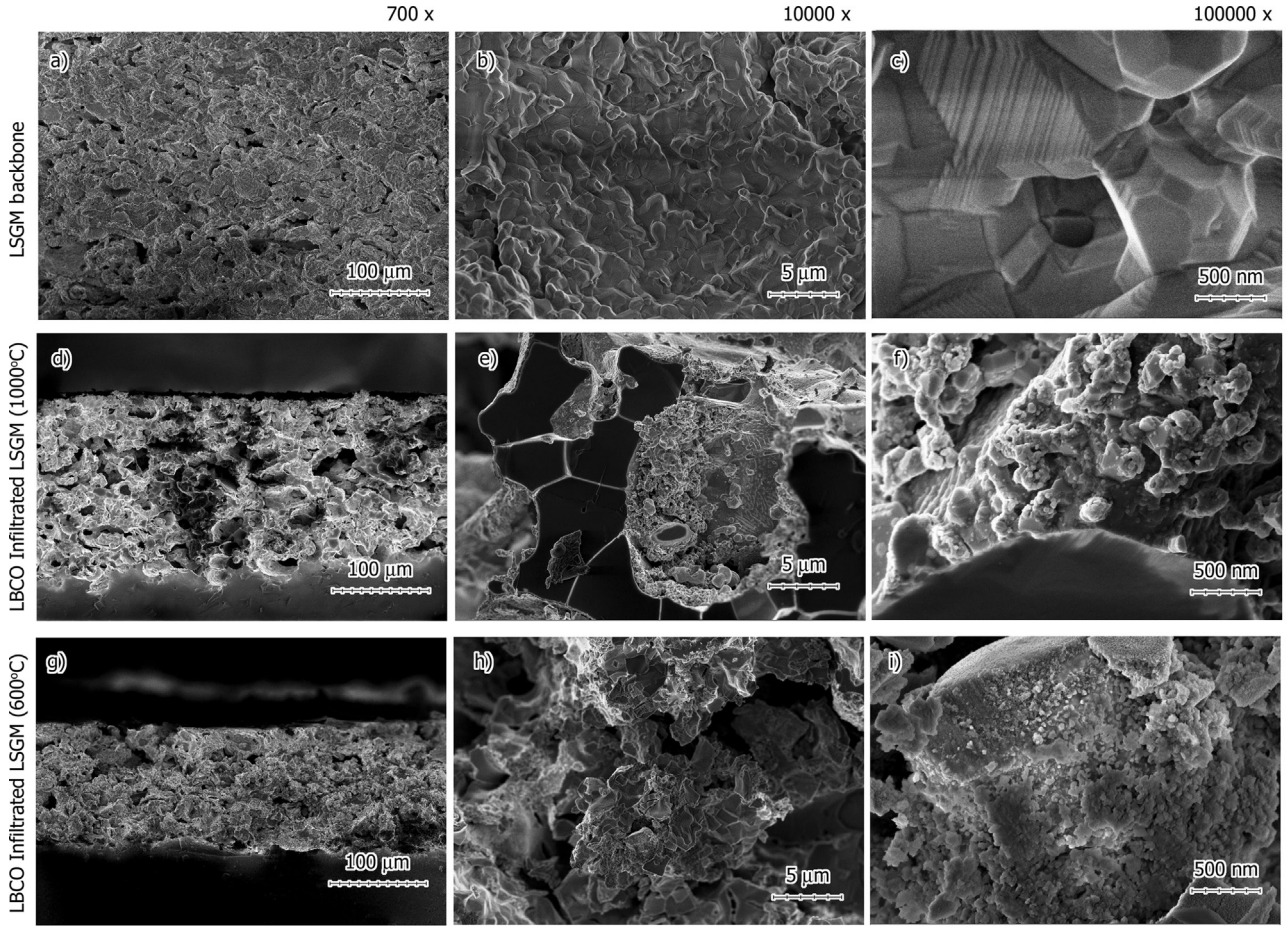

Fig. 3. SEM micrographs of the electrode cross section with different magnifications for LSGM backbone (a-c) and infiltrated LBC in LSGM backbone heat-treated at 1000 °C (d-f) and 600 °C (g-h).

sintered for 6 h at 1350 °C. The density of the LSGM scaffolds was obtained by measuring the dimensions and weight of a porous sintered pellet with the equal ratios of starch and LSGM using in the electrode. Thus, the density was estimated to be 33%. The precursor solution of LBC was prepared dissolving stoichiometric amounts of La_2O_3, previously dried overnight at 1000 °C, $BaCO_3$ and $Co(CH_3COO)_{2.4}H_2O$ in acetic acid. Small amounts of water and hydrogen peroxide were added to the solutions, which were refluxed at T ~ 80 °C until a clear solution was obtained. The solvents were then evaporated to obtain a solution with a concentration of 1.3 mol/l. A micro-liter syringe was used to infiltrate 50 µl of the LBC precursors solution into each side of the LSGM backbone. The final amount of infiltrated LBC into the electrodes was 14 wt%, calculated from the weight difference of the backbone before and after infiltration. A composite LBC/LSGM in a 1:1 wt ratio was prepared using materials obtained by the solid state reaction method. The ink for spray deposition was prepared by mixing the corresponding ceramic powder with ethanol, α-terpineol, polyvinyl butyral and polyvinyl pyrrolidone in 40:30:27:2:1 wt% ratio. The deposition onto the LSGM electrolyte was carried out using an airbrush. Subsequently the electrode was heat treated at T = 950 °C/1 h, in air.

The variation of the linear expansion with temperature was measured on cylindrical samples of approximately 5.0 mm diameter and 7–10 mm height, using a LINSEIS L75PT Series dilatometer. All the samples were heated up to 900 °C at 5 °C/min, and, after a 1 h dwell, were cooled to room temperature at a rate of 1 °C/min. They were then once again heated to 900 °C at a rate of 1 °C/min, in air. Experimental data were corrected using Al_2O_3 as a standard.

The impedance spectroscopy measurements were carried out in flowing air (100 ml/h), in the temperature range 400 °C ≤ T ≤ 900 °C by steps of 50 °C. The data acquisition was performed by an Autolab system PGSTAT-30 coupled to a module FRA2 in a frequency range of 1 MHz and 10^{-3} Hz. An AC signal of 10 mV was applied to the cell, under zero DC polarization. Pt grids, slightly pressed on the porous electrodes using a mullite tube, were used as current collectors. Impedance diagrams were analyzed using Z-view2 software [27]. The microstructure and thickness of the porous layers and interfaces were characterized by scanning electron microscopy (SEM) using a Zeiss Electron Beam SEM-Supra 40.

3. Results and discussion

3.1. Thermal expansion

Fig. 1 shows the $\Delta L/L_0$ vs. T curves for the LBC oxide, the composite LBC+LSGM in a 1:1 wt% ratio, the LBC-impregnated LSGM scaffolds and dense LSGM, being ΔL the change in length of the sample and L_0 its initial length. The total expansion values determined at various temperature are shown in Table 1. The TEC values obtained for LBC and LSGM were 26.4×10^{-6} K^{-1} and 12.0×10^{-6} K^{-1}, respectively, which are similar to those reported in the literature [13,28], while for the composite LBC+LSGM the TEC coefficient was 16.2×10^{-6} K^{-1}. In the case of the pellet prepared by impregnating LBC in the porous skeleton of LSGM the obtained value was 12.5×10^{-6} K^{-1}, slightly higher than that of the dense LSGM electrolyte. This result is similar to those reported for various cobaltites infiltrated electrodes [29]. Thus, the use of an electrode prepared with the infiltration technique virtually eliminates the mismatch in the linear expansion between the cobaltite and LSGM. Assuming there are no sintering effects in the linear

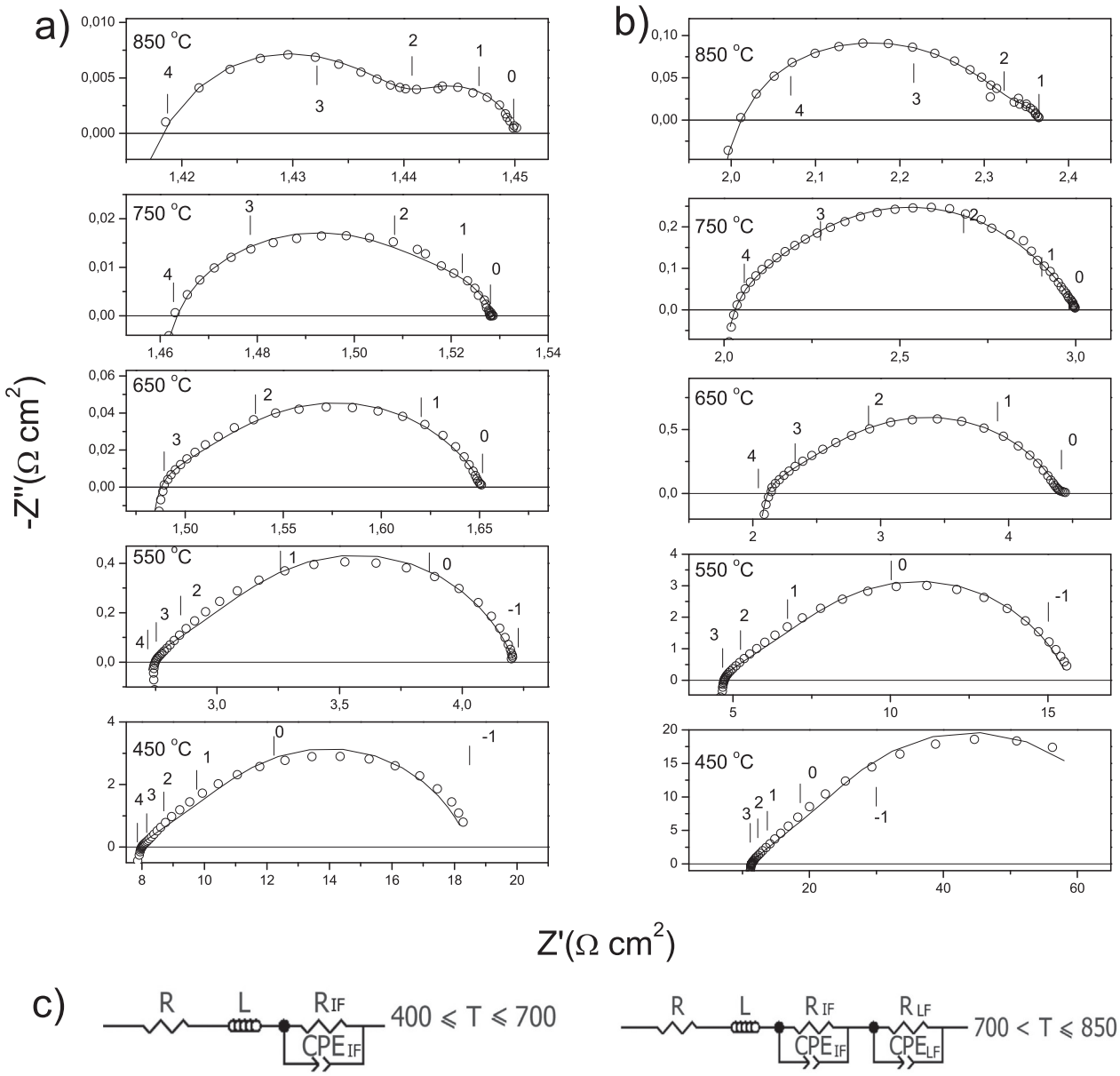

Fig. 4. Variation of the impedance spectra with temperature in the range 450 °C ≤ T ≤ 850 °C for a) LBC infiltrated in LSGM and b) LBC + LSGM composite electrodes. The solid line corresponds to the fit of the experimental data. The logarithm of the frequency is indicated in the Figure. Figure c shows the equivalent circuit used for fitting impedance data. The symbols correspond to the experimental and the solid line to the data fit by the equivalent circuit.

expansion data of our samples, no difference should be expected for the TEC value of the porous scaffold and the dense samples of LSGM. This effect is observed in Table 1 and Fig. 1, where a slight variation in the TEC value for the LBC infiltrated LSGM sample compared to LSGM, is observed.

3.2. Complex impedance

3.2.1. Thermal treatment of the infiltrated electrode

Fig. 2 shows the evolution of the complex impedance spectra measured at 600 °C, in air, after the symmetrical cell with infiltrated LBC electrodes being heat treated sequentially between 600 °C and 1000 °C. The polarization resistance (*Rp*) measured at 600 °C decreases as the heat-treatment temperature increases, reaching its minimum value, $Rp = 0.22\,\Omega\,cm^2$, when treated at 900 °C. This temperature is the same previously obtained for graded cathodes prepared with LBC and GDC [9]. The *Rp* value rapidly decreases as the heat treatment temperature increases up to 900 °C and slowly increases for T > 900 °C. Fig. 3a-c show SEM images of the LSGM scaffolds heat treated at 1350 °C with various magnifications, while Fig. 3d-f and g-i show the infiltrated LBC electrodes of the symmetrical cells heat treated at 900 and 600 °C, respectively. The electrodes were ~ 100 μm thick and uniform (see Fig. 3d and g). As seen from the SEM images, the pores of the LSGM skeleton are greater than 5 μm. The particle size was lower than 100 nm for the impregnated LBC heat treated at 600 °C, and lower than 500 nm for that heat treated at 900 °C. Noteworthy, the lowest Rp value was obtained for infiltrated cobaltite with larger particle size than those of the electrodes heat treated at T < 900 °C. This result indicates that not only large specific area but also connectivity between the cobaltite and the electrolyte are relevant parameters [8,9]. In addition, previous studies have shown that LBC cobaltite heat treated in the temperature range 600 °C ≤ T ≤ 800 °C is formed by a mixture of the cubic perovskite with a hexagonal phase that evolves to the cubic perovskite at 900 °C [7,9]. Thus, the lowest Rp value is due to the higher formation of the cubic phase fraction, good adhesion of LBC particles to the LSGM electrolyte backbone and a large specific area.

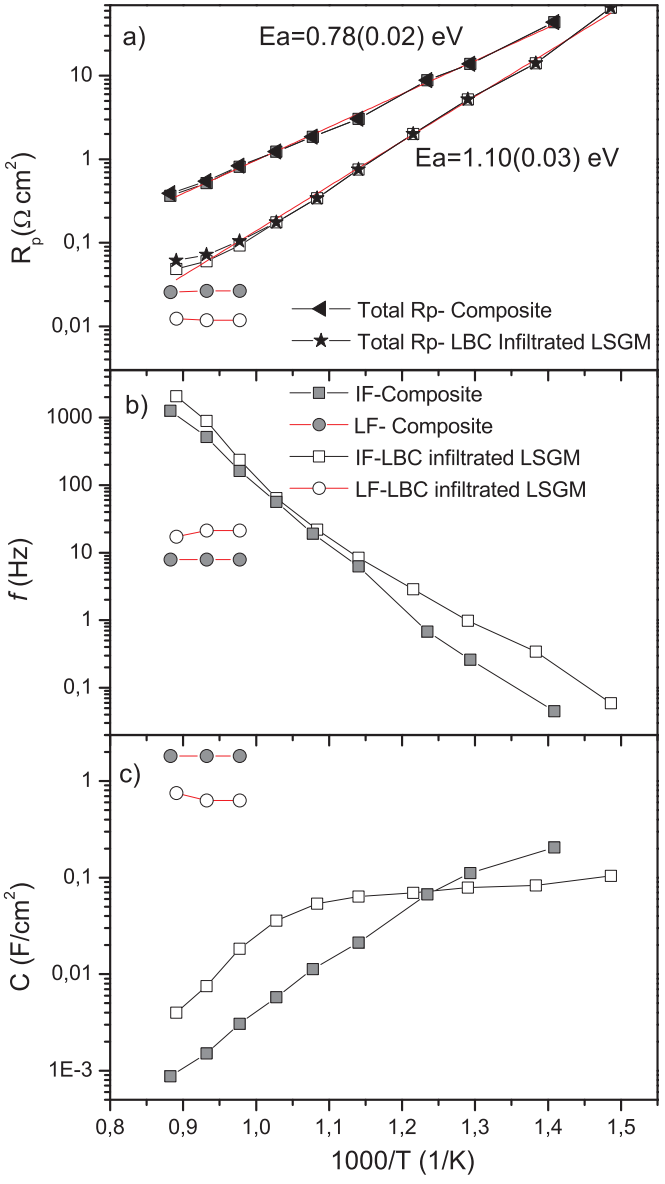

Fig. 5. a) Arrhenius plots of the polarization resistances Rp, R_{LF} and R_{IF} obtained for infiltrated LBC in LSGM backbone and composite LBC + LSGM electrodes. b) and c) display the Arrhenius plots for the apex frequency and the capacitance, respectively, for the IF and LF contributions of the impedance spectra.

Furthermore, infiltrated LBC particles require connectivity to achieve electronic percolation through the electrode. As was reported, the electrical conductivity of the LBC cubic phase is higher than 1000 S/cm, in air, at intermediate temperature [13,30]. This value is high compared to other cathodes such as $Ba_{0.5}Sr_{0.5}Co_{0.8}Fe_{0.2}O_{3-\delta}$ whose electrical conductivity value is < 40 S/cm [31]. On the other hand the formation of secondary phases due to the reaction of LBC with LSGM are expected at temperatures above T = 1100 °C [13].

3.2.2. ORR limiting processes for LBC infiltrated electrode

The identification of the limiting processes during the ORR at the cathode electrode was performed by complex impedance spectroscopy measurements. The impedance spectra supply information about the variation of several parameters related with the performance of the cathode of the SOFCs, which is very useful in order to design a suitable cathode material [32]. Impedance measurements were carried out in the temperature range 450 °C ≤ T ≤ 850 °C, while the oxygen partial

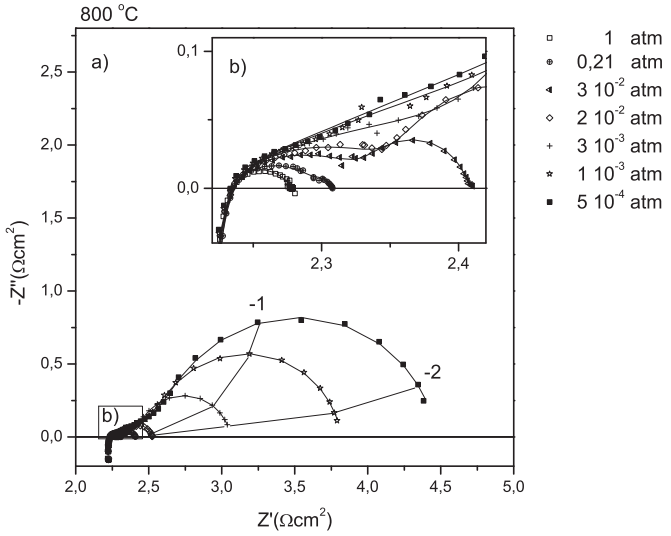

Fig. 6. Variation of the impedance spectra as a function of pO_2 at 800 °C for infiltrated LBC in LSGM electrode.

Table 2
Polarization resistance process and its associated parameter n for Rp = K pO_2^n.

Rp process	n
$O^-_{ad} + e^- + V_O^{\bullet\bullet} \leftrightarrow O_O^x$	− 0.25
$O_2 + 2e^- \leftrightarrow 2\,O^-_{ad}$	− 0.5
$O_2 \leftrightarrow O_{2,ad}$	− 1
O_2 gas diffusion	− 1

pressure (pO_2) range during measurements was varied in the $5 \times 10^{-4} \leq pO_2 \leq 1$ atm range. Fig. 4a and b show the impedance spectra for the LBC infiltrated LSGM backbone and a LBC-LSGM composite electrodes, respectively. The *Rp* value for the infiltrated LBC electrode was found to be lower than that of the composite LBC + LSGM electrode in the whole temperature range, being almost one order of magnitude lower at T ≥ 650 °C and about 5 times smaller at T ≤ 550 °C. The Nyquist plot of impedance spectra at low temperatures shows only one arc whose maximum frequency increases with temperature increment. This behavior was also found in other cathode materials, as we reported in previous works [9] with a apex frequency in the range 0.1–10^3 Hz. As described below, the apex frequency lower bound of this arc results somewhat lower than that reported in previous papers [9], however, as the electrochemical processes involved are the same we decided to keep the name of intermediate frequency (IF) used in previous works for this arc. At 750 °C ≤ T ≤ 850 °C a second arc appears in the low frequency range of the spectra. The behavior of this arc is similar to the contribution we denominated low frequency (LF) in previous papers [9], although the apex frequency (10–20 Hz) is slightly larger than that obtained in those works (2.5–3.5 Hz). Regardless of this behavior, we kept the name of this arc as LF contribution. The impedance spectra were analyzed by fitting the experimental data with an equivalent circuit consisting of a pure resistance (*R*) in series with an inductance (*L*) representing the resistance of the electrolyte and the inductance of the cables in the experimental setup, respectively. In addition, (R_i,CPE_i) elements formed by a resistance R_i in parallel with a constant phase element $CPE_i = 1/(B(j2\pi f)^p)$, where *B* is a constant, *p* a parameter that may change from $p = 1$ for a pure capacitor to $p = -1$ for a pure inductance, and *f* the frequency of the signal, were added depending on the temperature range, as indicated in Fig. 4c. For the temperature range 400 °C ≤ *T* ≤ 700 °C, we added the (R_{IF}, CPE_{IF}) element in series to describe the IF contribution, while for the temperature range 700 °C < T ≤ 850 °C the elements (R_{IF}, CPE_{IF}) and (R_{LF}, CPE_{LF}) were

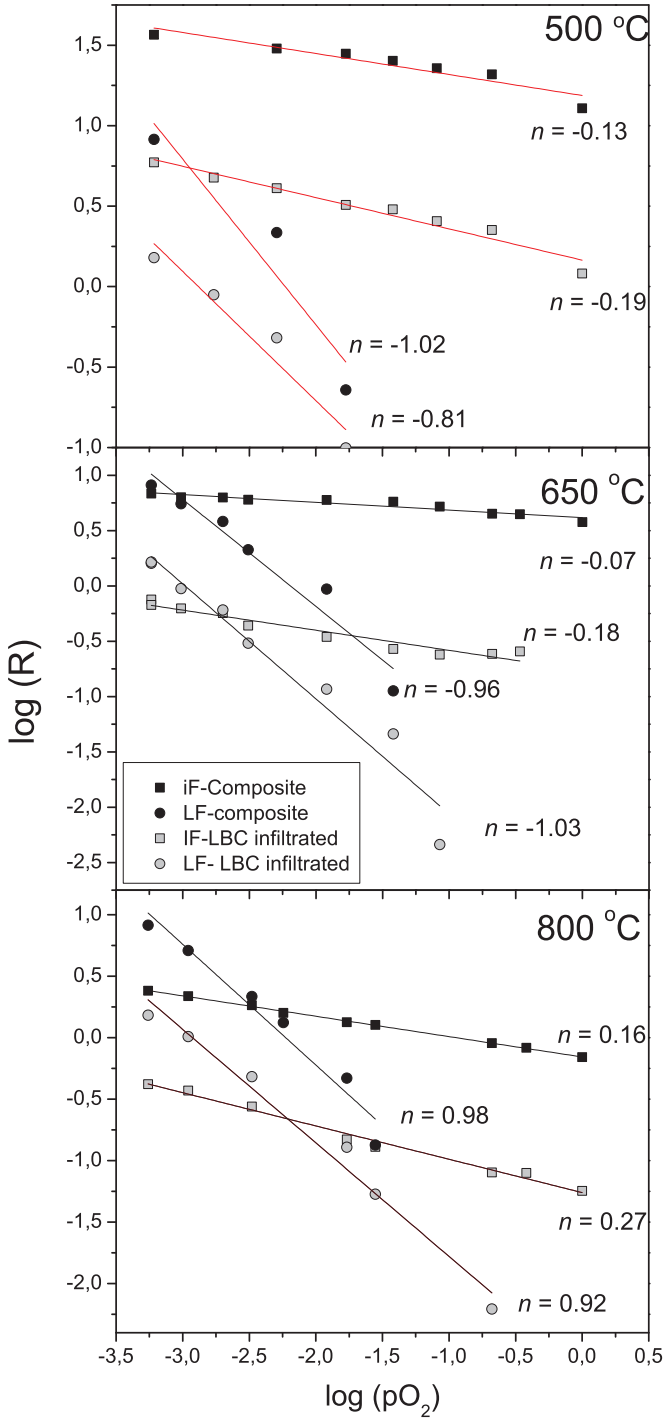

Fig. 7. Variation of Rp, R_{LF}, and R_{IF} as a function of pO_2 for infiltrated LBC in LSGM and composite LBC + LSGM electrodes at a) 500 °C, b) 650 °C, and c) 800 °C.

Table 3
Parameter *n*.

	T (°C)		
Cell-Process	500	650	800
Composite - IF	− 0.13 (0.02)	− 0.07 (0.01)	− 0.16 (0.01)
Infiltrated - IF	− 0.19 (0.02)	− 0.18 (0.02)	− 0.27 (0.02)
Composite - LF	− 1.02 (0.32)	− 0.96 (0.11)	− 0.98 (0.10)
Infiltrated - LF	− 0.81 (0.14)	− 1.03 (0.09)	− 0.92 (0.10)

added to reproduce the IF and LF contribution, respectively. The fit to the experimental data using these equivalent circuits are shown in Fig. 4a and b. The Arrhenius plots of the total polarization resistance Rp and those for each process R_i, the apex frequency f_i and the capacitance C_i with i = IF and LF obtained for the LBC impregnated and LBC + LSGM composite electrodes are shown in Fig. 5a-c. At low and medium temperatures the total polarization resistance is controlled by R_{IF} while at high temperature R_{LF} has a slight influence. Thus, the activation energy value (*Ea*) for Rp is the one obtained for the IF process for both electrodes, Ea ≈ 1.10 eV, which is in the range (1.06–1.20 eV) of the activation energy values reported by Zhan et. [18], using cobaltites ($La_{0.8}Sr_{0.2}CoO_{3-\delta}$, $La_{0.58}Sr_{0.4}Co_{0.2}Fe_{0.8}O_{3-\delta}$ and $SmBa_{0.5}Sr_{0.5}Co_{2.0}O_{5+\delta}$) infiltrated in ZrO_2 doped with Ce and Sc. It can be seen that R_{LF} shows little or no variation with temperature for both electrodes, as well as its apex frequency and capacitance, whose values remain in the ranges 10 Hz ≤ f_{LF} ≤ 20 Hz and 0.5 F/cm^2 ≤ C_{LF} ≤ 2 F/cm^2, respectively. On the other hand, the polarization resistance values for the IF contribution show a pronounced dependence on temperature, with the characteristic frequency varying from 0.05 to 2000 Hz when the temperature increases from 450 to 850 °C. The activation energies (*Ea*) for R_{IF} turned out to be 1.10 (0.02) and 0.78 (0.02) eV for the infiltrated and the composite electrode, respectively, as shown in Fig. 5a. These values, which represent the main contribution to the total polarization resistance *Rp*, are in the range of those reported in the literature [9,30,33]. Impedance measurements were performed at T = 500, 650 and 800 °C varying pO_2 for both the infiltrated LBC and the composite LBC + LSGM cathodes. The Nyquist diagrams at 800 °C and various pO_2 values for the infiltrated electrode are shown in Fig. 6. The analysis of the polarization resistance data performed with the power law:

$$R = K \times pO_2{}^n \quad (1)$$

where *n* is a parameter related to the species involved in the reaction and the process responsible for the polarization of the electrode. The electrochemical processes taking place during the oxygen reduction reaction at the cathode and the value of the parameter *n* for each of them are listed in Table 2 [9,33–35]. The value $n \approx -0.25$ is associated with the charge transfer and reduction of the adsorbed atomic oxygen followed by the incorporation of the oxygen ion at the electrode, $n \approx -0.5$ is related to the dissociation of the oxygen molecule at the electrode surface and finally a value of $n \approx -1$ is associated with the molecular adsorption of oxygen at the electrode surface [9,33–35]. Fig. 7 shows the variation of the polarization resistances R_{IF} and R_{LF} with pO_2 at various temperatures. In both cases, the polarization resistance decreases as the pO_2 increases, although the slope of the log (R_i) vs. log (pO_2) curves for $R_i = R_{LF}$ is clearly more negative than that for R_{IF}. The values for the parameter *n*, obtained from the linear fit of the log (R_i) vs. log (pO_2) data points, are listed in Table 3.

As mentioned above, the polarization resistance R_{LF} varies slightly with temperature, this is also true for the apex frequency and the capacitance whose values were in the ranges 5 ≤ *f* ≤ 20 Hz and 0.5 ≤ *C* ≤ 2 F/cm^2, respectively. Also, the parameter *n* in Eq. (1) for R_{LF} was systematically found to be close to − 1 (see Fig. 7 and Table 3) regardless of the temperature. Moreover, this value was obtained for both cathodes, the LBC-impregnated LSGM and the LBC + LSGM composite. These data suggest the LF contribution can be associated with the diffusion of oxygen in the gas phase through the electrode pores [9,33,34]. The R_{LF} value obtained for the infiltrated LBC in LSGM electrode, R_{LF} ≈ 0.01 Ω cm^2, is lower than the value obtained in this work for the composite LBC + LSGM electrode, R_{LF} ~ 0.03 Ω cm^2, and also lower than the R_{LF} reported in a previous work [9] for cathodes prepared with a composite LBC + GDC or with a configuration of graded composition of LBC and GDC [9]. This difference could be related to the larger pore size of the infiltrated electrode, where soluble starch was used as pore former, compared to that of the LBC + LSGM composite layer, where pores were formed by additives included in the formation of the ink

used for spray deposition (α-terpineol, polyvinyl butyral and polyvinyl pyrrolidone) [9] giving place to a more uniform and smaller pore size distribution compared with the case of the infiltrated electrode. In contrast, as we described above, the polarization resistance due to the IF arc was found to be thermally activated with an activation energy of 1.10 and 0.78 eV for the LBC infiltrated LSGM and LBC + LSGM composite electrodes, respectively. The apex frequency changes from 0.05 to 2000 Hz and the capacity from 1×10^{-3} to 0.2 F/cm^2 when the temperature increases from 450 to 850 °C. The values of the parameter n obtained from the slope of the log (R) vs. log (pO_2) curves using Eq. (1) were found in the range $-0.3 \leq n \leq -0.1$. For the composite LBC + LSGM electrode, the parameter n resulted -0.1, while for the infiltrated LBC electrode it was determined in the range $-0.18 \geq n \geq -0.27$ (see Table 3), which is close enough to $n = -0.25$ to associate the IF contribution with the charge transfer at the electrode surface for the reduction of the oxygen atom and the incorporation of the oxygen ion into the bulk (see Table 2). In the case of the LBC + LSGM composite electrode the parameter n turned out to be around -0.1, which indicates that the charge transfer process at the electrode/electrolyte interface coexists with the electronic charge transfer plus the oxygen ion incorporation at the electrode surface [33,36,37]. We speculate, this difference could be associated to a larger electrode/electrolyte interface area for the infiltrated electrode compared to the electrode prepared with the composite.

4. Conclusions

An infiltrated LBC in porous LSGM scaffold cathode was prepared. The optimum heat treatment temperature was T = 900 °C with a value of $Rp = 0.22\,\Omega\,cm^2$ at 600 °C. SEM microscopy showed that at T = 900 °C the particle size of the infiltrated LBC is < 500 nm. The infiltrated LBC suppress the mismatch in the linear expansion between the cobaltite $\alpha_{LBC} = 12.5 \times 10^{-6}\ K^{-1}$ and the electrolyte, $\alpha_{LSGM} = 12.0 \times 10^{-6}\ K^{-1}$. The limiting processes for the ORR were analyzed by complex impedance spectroscopy. Two processes were identified, these were denominated intermediate frequency (IF) and low frequency (LF), in agreement with previous works [9]. The polarization resistance of the LF process showed a slight dependence on temperature and the slope of the log (R_{LF}) vs log pO_2 data was n = − 1, which corresponds to the diffusion of the oxygen molecule in the pores of the electrode. For the infiltrated electrode R_{LF} turned out to be half the value obtained for the LBC-LSGM composite electrode, which could be associated to differences in the pore size among both electrodes. On the other hand, the behavior of the IF contribution suggests it is related, in the case of the infiltrated electrode, to the electronic charge transfer for oxygen reduction at the surface of the electrode and to its incorporation into the lattice and, to a mixture of the former processes and the charge transfer at the electrode/electrolyte interface, in the case of the composite electrode. Clearly, the polarization resistance of the infiltrated electrode LBC in LSGM is smaller than that of the electrode prepared with the composite LBC + LSGM, which suggests that mixed conductor oxide infiltration is a remarkable technique for preparing the cathode electrodes in SOFC.

Acknowledgements

The authors thank A. Prado for English revision of the manuscript. This work was supported by Consejo Nacional de Investigaciones Científicas y Técnicas (CONICET) and Agencia Nacional de Promoción Científica y Técnica (ANPCyT), Argentina, through PIP 112 2013 0100151 CO, and PICT 2013-1032, 2013-1587 and 2016-1921, respectively.

References

[1] N.Q. Minh, Ceramic fuel cells, J. Am. Ceram. Soc. 76 (1993) 563–588, http://dx.doi.org/10.1111/j.1151-2916.1993.tb03645.x.

[2] A.J. Jacobson, Materials for solid oxide fuel cells, Chem. Mater. 22 (2010) 660–674, http://dx.doi.org/10.1021/cm902640j.

[3] Z. Gao, L.V. Mogni, E.C. Miller, J.G. Railsback, S.A. Barnett, A perspective on low-temperature solid oxide fuel cells, Energy Environ. Sci. 9 (2016) 1602–1644, http://dx.doi.org/10.1039/C5EE03858H.

[4] Z. Shao, S.M. Haile, A high-performance cathode for the next generation of solid-oxide fuel cells, Nature 431 (2004) 170–173, http://dx.doi.org/10.1038/nature02863.

[5] J.-H. Kim, F. Prado, A. Manthiram, Characterization of $GdBa_{1-x}Sr_xCo_2O_{5+\delta}$ ($0 \leq x \leq 1.0$) double perovskites as cathodes for solid oxide fuel cells (B1023–B1028), J. Electrochem. Soc. 155 (2008), http://dx.doi.org/10.1149/1.2965792.

[6] J.-H. Kim, L. Mogni, F. Prado, A. Caneiro, J.A. Alonso, A. Manthiram, High temperature crystal chemistry and oxygen permeation properties of the mixed ionic–electronic conductors $LnBaCo_2O_{5+\delta}$ (Ln = Lanthanide), J. Electrochem. Soc. 156 (2009) B1376, http://dx.doi.org/10.1149/1.3231501.

[7] C. Setevich, L. Mogni, A. Caneiro, F. Prado, Characterization of the $La_{1-x}Ba_xCoO_{3-\delta}$ ($0 \leq x \leq 1$) system as cathode material for IT-SOFC, J. Electrochem. Soc. 159 (2012) B73, http://dx.doi.org/10.1149/2.043201jes.

[8] C.F. Setevich, L.V. Mogni, A. Caneiro, F.D. Prado, Optimum cathode configuration for IT-SOFC using $La_{0.4}Ba_{0.6}CoO_3$-d and $Ce_{0.9}Gd_{0.1}O_{1.95}$, Int. J. Hydrog. Energy 37 (2012) 14895–14901, http://dx.doi.org/10.1016/j.ijhydene.2012.01.155.

[9] C. Setevich, F. Prado, A. Caneiro, Study of the electrode polarization resistance of cobaltites with high Ba content as cathode for IT-SOFC, J. Electrochem. Soc. 164 (2017) F759–F767, http://dx.doi.org/10.1149/2.0681707jes.

[10] H. Gu, H. Chen, L. Gao, L. Guo, Electrochemical properties of $LaBaCo_2O_{5+}$d-$Sm_{0.2}Ce_{0.8}O_{1.9}$ composite cathodes for intermediate-temperature solid oxide fuel cells, Electrochim. Acta 54 (2009) 7094–7098, http://dx.doi.org/10.1016/j.electacta.2009.07.040.

[11] Q. Zhou, F. Wang, Y. Shen, T. He, Performances of $LnBaCo_2O_{5+x}$-$Ce_{0.8}Sm_{0.2}O_{1.9}$ composite cathodes for intermediate-temperature solid oxide fuel cells, J. Power Sources 195 (2010) 2174–2181, http://dx.doi.org/10.1016/j.jpowsour.2009.10.062.

[12] S. Choi, S. Park, J. Kim, T.H. Lim, J. Shin, G. Kim, Electrochemical properties of an ordered perovskite $LaBaCo_2O_{5\ +}$d-$Ce_{0.9}Gd_{0.1}O_2$.d composite cathode with strontium doping for intermediate-temperature solid oxide fuel cells, Electrochem. Commun. 34 (2013) 5–8, http://dx.doi.org/10.1016/j.elecom.2013.04.016.

[13] J.H. Kim, A. Manthiram, $LnBaCo_2O_5$ oxides as cathodes for intermediate-temperature solid oxide fuel cells, J. Electrochem. Soc. 155 (2008) 385–390, http://dx.doi.org/10.1149/1.2839028.

[14] R. Li, L. Ge, H. Chen, L. Guo, Preparation and performance of triple-layer graded $LaBaCo_2O_{5+\delta}$–$Ce_{0.8}Sm_{0.2}O_{1.9}$ composite cathode for intermediate-temperature solid oxide fuel cells, Electrochim. Acta 85 (2012) 273–277, http://dx.doi.org/10.1016/j.electacta.2012.08.071.

[15] Z. Liu, B. Liu, D. Ding, M. Liu, F. Chen, C. Xia, Review Fabrication and modification of solid oxide fuel cell anodes via wet impregnation/infiltration technique, J. Power Sources 237 (2013) 243–259, http://dx.doi.org/10.1016/j.jpowsour.2013.03.025.

[16] D. Ding, X. Li, S.Y. Lai, K. Gerdes, M. Liu, Enhancing SOFC cathode performance by surface modification through infiltration, Energy Environ. Sci. 7 (2014) 552, http://dx.doi.org/10.1039/c3ee42926a.

[17] A.J. Samson, M. Søgaard, P. Hjalmarsson, J. Hjelm, N. Bonanos, S.P.V. Foghmoes, T. Ramos, Durability and performance of high performance infiltration cathodes, Fuel Cells 13 (2013) 511–519, http://dx.doi.org/10.1002/fuce.201200183.

[18] W. Zhan, Y. Zhou, T. Chen, G. Miao, X. Ye, J. Li, Z. Zhan, S. Wang, Z. Deng, Long-term stability of infiltrated $La_{0.8}Sr_{0.2}CoO_{3-\delta}$, $La_{0.58}Sr_{0.4}Co_{0.2}Fe_{0.8}O_{3-\delta}$ and $SmBa_{0.5}Sr_{0.5}Co_{2.0}O_{5+\delta}$ cathodes for low temperature solid oxide fuel cells, Int. J. Hydrog. Energy 40 (2015) 16532–16539, http://dx.doi.org/10.1016/j.ijhydene.2015.08.073.

[19] A. Samson, M. Søgaard, R. Knibbe, N. Bonanos, High performance cathodes for solid oxide fuel cells prepared by infiltration of $La_{0.6}Sr_{0.4}CoO_{3-\delta}$ into Gd-doped ceria, J. Electrochem. Soc. 158 (2011) B650, http://dx.doi.org/10.1149/1.3571249.

[20] Da Han, X. Liu, F. Zeng, J. Qian, T. Wu, Z. Zhan, A micro-nano porous oxide hybrid for efficient oxygen reduction in reduced-temperature solid oxide fuel cells, Sci. Rep. 2 (2012) 1–5, http://dx.doi.org/10.1038/srep00462.

[21] S.P. Jiang, Nanoscale and nano-structured electrodes of solid oxide fuel cells by infiltration: advances and challenges, Int. J. Hydrog. Energy 37 (2012) 449–470, http://dx.doi.org/10.1016/j.ijhydene.2011.09.067.

[22] Z. Zhan, D.M. Bierschenk, J.S. Cronin, S.A. Barnett, A reduced temperature solid oxide fuel cell with nanostructured anodes, Energy Environ. Sci. 4 (2011) 3951, http://dx.doi.org/10.1039/c1ee01982a.

[23] Z. Zhan, D. Han, T. Wu, X. Ye, S. Wang, T. Wen, S. Cho, S.A. Barnett, A solid oxide cell yielding high power density below 600 °C, RSC Adv. 2 (2012) 4075, http://dx.doi.org/10.1039/c2ra20413d.

[24] Y. Wang, H. Zhang, F. Chen, C. Xia, Electrochemical characteristics of nano-structured $PrBaCo_2O_{5+x}$ cathodes fabricated with ion impregnation process, J. Power Sources 203 (2012) 34–41, http://dx.doi.org/10.1016/j.jpowsour.2011.11.069.

[25] D. Chen, R. Ran, Z. Shao, Assessment of $PrBaCo_2O_{5+}$d + $Sm_{0.2}Ce_{0.8}O_{1.9}$ composites prepared by physical mixing as electrodes of solid oxide fuel cells, J. Power Sources 195 (2010) 7187–7195, http://dx.doi.org/10.1016/j.jpowsour.2010.05.018.

[26] D. Han, H. Wu, J. Li, S. Wang, Z. Zhan, Nanostructuring of $SmBa_{0.5}Sr_{0.5}Co_2O_{5+\delta}$ cathodes for reduced-temperature solid oxide fuel cells, J. Power Sources 246 (2014) 409–416, http://dx.doi.org/10.1016/j.jpowsour.2013.07.113.

[27] D. Johnson, ZView and ZPlot: a Software Program for IES Analysis, 2002.

[28] J.W. Stevenson, K. Hasinska, N.L. Canfield, T.R. Armstrong, Influence of cobalt and iron additions on the electrical and thermal properties of $(La,Sr)(Ga,Mg)O_{3-\delta}$, J. Electrochem. Soc. 147 (2000) 3213, http://dx.doi.org/10.1149/1.1393885.

[29] F. Wang, D. Chen, Z. Shao, $Sm_{0.5}Sr_{0.5}CoO_{3-\delta}$-infiltrated cathodes for solid oxide fuel cells with improved oxygen reduction activity and stability, J. Power Sources 216 (2012) 208–215, http://dx.doi.org/10.1016/j.jpowsour.2012.05.068.

[30] D. Garcés, C.F. Setevich, A. Caneiro, G.J. Cuello, L. Mogni, Effect of cationic order–disorder on the transport properties of $LaBaCo_2O_{6-\delta}$ and $La_{0.5}Ba_{0.5}CoO_{3-\delta}$ perovskites, J. Appl. Crystallogr. 47 (2014) 325–334, http://dx.doi.org/10.1107/S1600576713031233.

[31] S. Li, Z. Lü, X. Huang, W. Su, Thermal, electrical, and electrochemical properties of Nd-doped $Ba_{0.5}Sr_{0.5}Co_{0.8}Fe_{0.2}O_{3-\delta}$ as a cathode material for SOFC, Solid State Ion. 178 (2008) 1853–1858, http://dx.doi.org/10.1016/j.ssi.2007.11.016.

[32] Q.A. Huang, R. Hui, B. Wang, J. Zhang, A review of AC impedance modeling and validation in SOFC diagnosis, Electrochim. Acta 52 (2007) 8144–8164, http://dx.doi.org/10.1016/j.electacta.2007.05.071.

[33] L. Mogni, N. Grunbaum, F. Prado, A. Caneiro, Oxygen reduction reaction on ruddlesden–popper phases studied by impedance spectroscopy, J. Electrochem. Soc. 158 (2011) B202, http://dx.doi.org/10.1149/1.3511770.

[34] Y. Takeda, Cathodic polarization phenomena of perovskite oxide electrodes with stabilized zirconia, J. Electrochem. Soc. 134 (1987) 2656, http://dx.doi.org/10.1149/1.2100267.

[35] Z. Gao, X.M. Liu, B. Bergman, Z. Zhao, Investigation of oxygen reduction reaction kinetics on $Sm_{0.5}Sr_{0.5}CoO_{3-\delta}$ cathode supported on $Ce_{0.85}Sm_{0.075}Nd_{0.075}O_{2-\delta}$ electrolyte, J. Power Sources 196 (2011) 9195–9203, http://dx.doi.org/10.1016/j.jpowsour.2011.07.012.

[36] M.J. Escudero, A. Aguadero, J.A. Alonso, L. Daza, A kinetic study of oxygen reduction reaction on La_2NiO_4 cathodes by means of impedance spectroscopy, J. Electroanal. Chem. 611 (2007) 107–116, http://dx.doi.org/10.1016/j.jelechem.2007.08.006.

[37] S. Pang, X. Jiang, X. Li, Z. Su, H. Xu, Q. Xu, C. Chen, Characterization of cation-ordered perovskite oxide $LaBaCo_2O_{5+\delta}$ as cathode of intermediate-temperature solid oxide fuel cells, Int. J. Hydrog. Energy 37 (2012) 6836–6843, http://dx.doi.org/10.1016/j.ijhydene.2012.01.056.